Songklanakarin J. Sci. Technol.
48 (1), e20260107, Jan. – Feb. 2026

http://www.sjst.psu.ac.th

*Original Article*

# Development and empirical analysis of a 3D haptic joystick utilizing three rotary MR brakes

Le Hai Zy Zy, Vu Van Bo, Diep Bao Tri*, and Nguyen Quoc Hung*

*Faculty of Mechanical Engineering, Industrial University of Ho Chi Minh City, Ho Chi Minh City, 727000 Vietnam*

Received: 5 July 2023; Revised: 17 May 2025; Accepted: 29 September 2025

## Abstract

This study focuses on the development and evaluation of a 3D haptic system employing three Magnetorheological Brakes (MRBs) integrated through a gimbal mechanism. A comprehensive literature review was conducted to design a 3D haptic joystick configuration capable of delivering force feedback using MRF actuators. The gimbal mechanism was integrated with the three MRBs to generate force feedback in X, Y, and Z directions. The MRBs were optimally designed and modeled using the finite element method and the Bingham plastic rheological model, aiming to reduce both mass and production costs. Particle Swarm Optimization was employed to obtain optimized geometry of the MRBs. A prototype 3D haptic joystick was manufactured and experimentally tested to assess its force feedback capabilities. This research holds promise for advancing future studies on force feedback in remote control systems, particularly in the context of Master-Slave systems.

**Keywords**: feedback force, 3D haptic joystick, magnetorheological fluid (MRF), magnetorheological brake (MRB), particle swarm optimization (PSO)

## 1. Introduction

Telemanipulators are increasingly important in reality, especially in hard environments where robots, such as adventure robots, are used to perform various tasks. One of the primary challenges in remote control systems is the absence of force and torque feedback, which limits the operator's ability to perceive and respond to interactions. This results in decreased system accuracy and flexibility. To address this issue, integrating telemanipulator systems with force feedback to the operator, known as remote haptic systems, is highly significant. In recent years, magnetorheo logical fluid (MRF) has emerged as a promising material for various applications, including clutches, brakes, and dampers, due to its unique properties, such as significant changes in rheological characteristics under an external magnetic field (Kang, Kim, Jung, & Choi, 2022; Nguyen, Hiep, Duy, & Choi, 2016; Nguyen, Thang, & Nguyen, 2018).

*Corresponding author
Email address: diepbaotri@iuh.edu.vn, nguyenquochung@iuh.edu.vn

Previous studies have focused on haptic systems using MR actuators, or MR haptic systems. For instance, Yamaguchi, Furusho, Kimura, and Koyanagi (2004) proposed a multi-DOF haptic system using MR actuators to simulate 2D virtual forces, but each MR brake was large (170 mm × 120 mm, 4 kg) and produced only 10 N torque with low off-state force. Winter and Bouzit (2007) developed a force feedback glove with a linear MR brake generating 6 N force, though with high off-state force (1.5 N) and large size. Bullion and Gurocak (2009) created a 3-DOF haptic glove with three rotating MR brakes for the thumb, index, and middle fingers, producing 17 N total force with compact brakes (D=25 mm, L=15 mm). Senkal and Gurocak (2009) experimentally validated a joystick achieving 3.7 Nm torque without disk-shaped brakes by using an MR spherical brake as a multi-DOF actuator. However, high off-state torque caused undesirable friction and reduced reversibility. Nguyen, Oh, and Choi (2012) designed a 2-DOF haptic master with bidirectional MR actuators, eliminating friction but yielding only 1.2 Nm torque; increasing actuator size for higher torque was impractical. Nguyen, Choi, Lee, and Han (2013) studied a 3D haptic gripper using MR brakes with small mass and off-state torque, but no validation experiment was conducted. Oh,

Choi, and Choi (2014) designed a 4-DOF MR haptic master for robotic surgery, combining a 2-DOF MR bidirectional clutch with a 2-DOF MR clutch. Its 2.33 Nm maximum torque was affected by a large joystick mass, reducing feedback due to gravity and inertia. Choi, Kim, Park, and Choi (2015) developed a master force feedback system using MR clutches and brake for tumor cutting. The haptic feedback closely matched force sensor data on the slave robot. The MR clutch reduced initial friction torque better than the MR brake but required more space, was harder to control, and had coil-related magnetic bottlenecks. Kim, Kim, Park, and Choi (2016) continued with tissue incision simulations, confirming similar feedback results. Coil design was improved, but the system's size still affected motion and feedback accuracy due to gravity on the Z-axis. Diep, Nguyen, Kim, and Choi (2020) have evaluated the performance of a 3D joystick with two bidirectional MR clutches and linear MRB. The experimental results were that the maximum feedback forces $F_x$ and $F_y$ are about 20N. However, the feedback of $F_z$ is not reflected fully in the system due to the off-state of linear MRB being quite high, about 5N.

Although numerous studies have explored MR haptic systems, previous research on MR actuators for these systems is limited and insufficient. Most efforts have primarily focused on actuator geometry and control mechanisms, neglecting critical aspects such as mitigating the magnetic field "bottleneck" issue and minimizing the mass of MR actuators. Additionally, the force feedback components remain interdependent, making axis-specific evaluation difficult. To address this, this study proposes a 3D haptic joystick with three rotary MR brakes. This design enables independent axis feedback, reduces magnetic bottlenecks, simplifies kinematics, and improves force feedback measurement accuracy. In section 2, configuration and working principle of the proposed 3D haptic joystick is presented, and the finite element method is employed in the next section to solve the magnetic circuits of the MR brake. Mathematical models of the MR brakes, such as induced torque and off-state torque, are built in section 3. Section 4 formulates the objective problem to minimize the MR brake's mass based on analyzing the mathematical models mentioned above. Optimal solution is then obtained, and a prototype of the optimized joystick is fabricated. Finally, experimental work is implemented in section 5 to validate the proposed design.

## 2. The 3D Haptic Joystick Featuring Three MR Brakes

Figure 1a shows configuration of the proposed 3D haptic joystick. Three MR brakes (MRBs) named MRB01, MRB02, and MRB03 are utilized to provide force feedback for each rotational motion. The shafts of MRB01 and MRB02 are respectively connected to X and Y axes of the gimbal mechanism while the shaft of MRB03 is connected to the gimbal frame of the gimbal. The rotation angles of the proposed 3D joystick are determined by the encoder placed on the opposite side of each MRB's shaft. MRB01 and MRB02 are fixed on the two rotational frames of the gimbal mechanism to represent the *X* and *Y*-axis rotation angles of the system, respectively. Moreover, MRB03 is fixed on the gimbal frame and baseplate to represent the *Z*-axis rotation angle of the proposed haptic system. The output torque of the MRBs is determined by a 3D force sensor located between the handle and knob of the joystick. The position of the operation knob is calculated from the measured angles of the encoders, and then the moment arm of the system is calculated from the knob's position. As a result, the 3D feedback force components F1, F2, and F3 can be achieved through the braking torque produced by the corresponding MRBs. In this research, angular working ranges for the *X* and *Y*-axis rotations are ±65° and ±57°, respectively, while the *Z*-axis rotation has a full circle range of 360°. A counterweight is employed to balance the handle's rotation along the *Y*-axis.

The MR brake with a tooth-shaped rotor proposed in this study for the 3D haptic joystick is depicted in Figure 1b. As illustrated in Figure 1b, the magnetic brake disc is attached to the flange of the nonmagnetic shaft, which is inserted into the magnetic brake housing. The space between the disc and the brake housing is filled with MR fluid. To generate magnetic flux passing through the MRF gap, two magnetic coils are located on each side of the brake housing. It should be mentioned that the coils of the brake are subjected to currents in the opposite directions.

To analyze the magnetic circuit of the proposed MRB, the finite element method (FEM) is utilized, which is incorporated in ANSYS APDL. Figure 2a illustrates the FEM using the axisymmetric element - PLANE 13 to construct the magnetic circuit of the MRB. The permeability of 1.0 (equivalent to air permeability) is used for MRB components such as the shaft (made of non-magnetic stainless steel) and the coil (made of copper), while the B-H curve of C45 steel is employed for the magnetic components (such as the housing and disc). Furthermore, the MRF-132DG made by Lord Cooperation is utilized in this study, and the magnetic characteristics of the MRF are estimated using the empirical formula given below (Varela-Jiménez, Vargas-Luna, Cortés-Ramírez, & Song, 2015):

$$B = 1.91 \cdot \Phi^{1.133}\left[1 - exp\left(-10.97 \cdot \mu_0 \cdot H\right)\right] + \mu_0 \cdot H \qquad (1)$$

Here $B$ and $H$ are respectively the magnetic flux density (*Tesla*) and magnetic flux intensity (*A/m*); the permeability vacuum $\mu_0 = 4\pi \cdot 10^{-7}$ is ; the volume fraction of iron in the MRF is $\Phi$.

Furthermore, Figure 2b illustrates the magnetic flux lines in the MRB simulated using ANSYS APDL. It is noted that that the tooth-shaped corresponding surfaces of the disc and housing create a large contact area between the MRF and the disc. This configuration is expected to enhance the induced torque and alleviate the bottleneck phenomenon that is inherent in MRBs.

## 3. Modeling of MRB and Kinematics of the 3D Joystick

The rheological behavior of the MRF utilized in this study is approximated by a Bingham rheological model, in addition, a linear velocity distribution of MRF in the gap is also assumed. The output torque of the MRB shown in Figure 1b can be estimated as follows (Nguyen & Choi, 2012):

$$T_b = 2\left(\sum_{i=0,2,4,6,8,10} T_{Ei} + \sum_{j=1,3,5,7,9} T_{Ij} + T_s\right) + T_c \qquad (2)$$

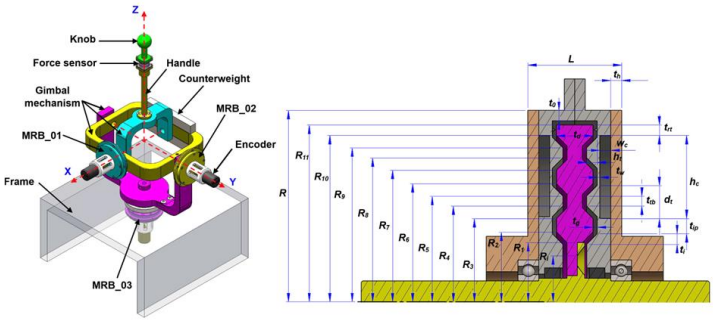


(a) CAD model of the proposed 3D haptic joystick

(b) Configuration and dimension of the proposed MRB

Figure 1. Configuration of the 3D haptic joystick and MRB

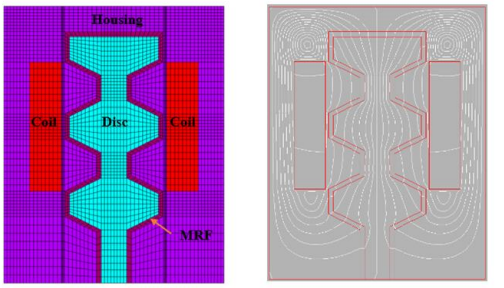


(a) Finite element model (b) Simulated magnetic flux lines

Figure 2. Simulation of the magnetic circuit of MRB

Where, $T_{Ei}$ is frictional torque induced by MRF in the vertical duct $E_i$; $T_{Ij}$ is frictional torque inducted by MRF in the inclined duct $I_j$; $T_c$ is frictional torque caused by MRF in the annular duct that is acting on the cylindrical face of the disc; and $T_s$ is the frictional torque of lip-seal. It can be noted that the frictional torque of bearing is neglected in this study. Additionally, the frictional torques $T_{Li}$, $T_{Ij}$, $T_c$ and $T_s$ are determined as follows.

$$T_{Ei} = \frac{\pi\mu_{Ei}R_{i+1}^4}{2d}\left[1-\left(\frac{R_i}{R_{i+1}}\right)^4\right]\Omega + \frac{2\pi\tau_{yEi}}{3}\left(R_{i+1}^3 - R_i^3\right); i = 0,2,4,6,8,10 \quad (3)$$

$$T_{Ij} = 2\pi\left(R_j^2 l + R_j l^2 \sin\varphi + \frac{1}{3}l^3\sin^2\varphi\right)\tau_{ylj} + \frac{l\Omega}{2d}\pi\mu_{lj}\left(4R_j^3 + 6R_i^2 l\sin\varphi + 4R_j l^2\sin^2\varphi + l^3\sin^3\varphi\right); j = 1,3,5,7,9 \quad (4)$$

$$T_c = 2\pi R_{11}^2 b\tau_{yc} + \mu_c\frac{\Omega R_{11}}{d} \quad (5)$$

$$T_s = 0.65(2R_s)^2\Omega^{1/3} \quad (6)$$

Here, $R_i$ and $R_j$ are respectively the radiuses of $i^{th}$ and $j^{th}$ points in the disc profile of the MRB depicted in Figure 1b; $\varphi$ and $l$ are the angle and length of the inclined duct; $R_s$ is the radius of sealing shaft measured in inches; $\tau_{yEi}$, $\tau_{ylj}$, $\tau_{yc}$ are respectively the yield stress of the MRF in the vertical duct $E_i$, the inclined duct $I_j$, and the annular duct, while $\mu_{Ei}$, $\mu_{lj}$, $\mu_c$ are the corresponding post-yield viscosities of the MRF. $\Omega$ is the angular speed of the brake shaft.

It is noteworthy that rheological properties of MRF such as the yield stress and the post-yield viscosity depend on the induced magnetic flux density across the MRF duct, and can be approximately estimated as follows (Nguyen & Choi, 2012):

$$\tau_y = \tau_{y\infty} + \left(\tau_{y0} - \tau_{y\infty}\right)\left(2e^{-B\alpha_{\tau y}} - e^{-2B\alpha_{\tau y}}\right)$$
$$\mu = \mu_\infty + \left(\mu_0 - \mu_\infty\right)\left(2e^{-B\alpha_\mu} - e^{-2B\alpha_\mu}\right) \quad (7)$$

Here the yield stress and the post-yield viscosity of the MRF at zero applied field are $\tau_{y0}$ and $\mu_0$, respectively; the yield stress and the post-yield viscosity of the MRF at the saturated magnetic flux density are respectively $\tau_{y\infty}$ and $\mu_\infty$; $B$ is the induced magnetic flux density ($T$); $\alpha_{\tau y}$ and $\alpha_\mu$ are respectively the saturation moment index of the yield stress and viscosity. Besides, the commercial MRF made by Lord Corporation, MRF132-DG, is employed in this study. Thus, the rheological properties of this MRF are presented as follows (Nguyen & Choi, 2012):

$$\mu_0 = 0.1pa\cdot s; \mu_\infty = 3.8pa\cdot s; \alpha_{\tau_y} = 2.9T^{-1};$$
$$\alpha_\mu = 4.5T^{-1}; \tau_{y_0} = 15pa; \tau_\infty = 40000\,pa.$$

Kinematic schematic of the 3D haptic joystick is presented in Figure 3.

From the figure, the Denavit – Hartenberg (*D-H*) table for the joystick is derived and shown in Table 1.

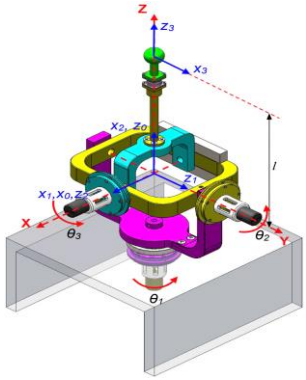


Figure 3. Coordinate systems of the proposed 3D haptic joystick ($X_3$=$Z_1$)

Table 1. *D-H* table of the 3D joystick

| Frame (*i*) | Denavit-Hartenberg table | | | |
|---|---|---|---|---|
| | $a_{i-1}$ | $\alpha_{i-1}$ | $d_i$ | $\theta_i$ |
| 1 | 0 | π/2 | 0 | $\theta_1$ |
| 2 | 0 | π/2 | 0 | $\theta_2$ |
| 3 | 0 | π/2 | 0 | $\theta_3$ |

From *D-H* table, transformation matrix of 3D haptic joystick is as follows:

$$ {}^{0}_{3}T = {}^{0}_{1}T \times {}^{1}_{2}T \times {}^{2}_{3}T \tag{8} $$

where, $ {}^{i}_{i+1}T = \begin{bmatrix} c\theta_i & -s\theta_i c\alpha_i & s\theta_i s\alpha_i & a_i \cdot c\theta_i \\ s\theta_i & c\theta_i c\alpha_i & c\theta_i s\alpha_i & a_i \cdot s\theta_i \\ 0 & s\alpha_i & c\alpha_i & d_i \\ 0 & 0 & 0 & 1 \end{bmatrix}$ ; *s = sin(); c = cos()*

The position of the operation knob is determined by using forward kinematics method as follows:

$$ r_p = {}^{0}_{3}T \times \begin{bmatrix} 0 \\ 0 \\ l \\ 1 \end{bmatrix} = \begin{bmatrix} l\,c\theta_3 s\theta_1 - c\theta_1 c\theta_2 s\theta_3 \\ -lc\theta_1 c\theta_3 + c\theta_2 s\theta_1 s\theta_3 \\ l s\theta_2 s\theta_3 \\ 1 \end{bmatrix}; \; s = sin(); \; c = cos() \tag{9} $$

The following equation can be utilized to determine the relationship between actuating torque ($T$) and force ($F$) from the acting torque at the operation knob:

$$ \begin{bmatrix} T_x \\ T_y \\ T_z \end{bmatrix} = J^T(\theta) \begin{bmatrix} F_x \\ F_y \\ F_z \end{bmatrix} \tag{10} $$

Here, $J(\theta)$ is Jacobian matrix depending on the angles ($\theta_1$, $\theta_2$, $\theta_3$); $T_x$, $T_y$, and $T_z$ are respectively induced torque of MRB according to *X*, *Y*, and *Z*; $F_x$, $F_y$, $F_z$ are respectively force of the 3D joystick in the *X*, *Y*, and *Z* directions.

$$ J(\theta) = \begin{bmatrix} \frac{\partial r_{p11}}{\partial \theta_1} & \frac{\partial r_{p11}}{\partial \theta_2} & \frac{\partial r_{p11}}{\partial \theta_3} \\ \frac{\partial r_{p21}}{\partial \theta_1} & \frac{\partial r_{p21}}{\partial \theta_2} & \frac{\partial r_{p21}}{\partial \theta_3} \\ \frac{\partial r_{p31}}{\partial \theta_1} & \frac{\partial r_{p31}}{\partial \theta_2} & \frac{\partial r_{p31}}{\partial \theta_3} \end{bmatrix} = \begin{bmatrix} l\cdot(c\theta_1 c\theta_3 + c\theta_2 s\theta_1 s\theta_3) & l\cdot(c\theta_1 s\theta_2 s\theta_3) & -l\cdot(s\theta_1 s\theta_3 + c\theta_1 c\theta_2 c\theta_3) \\ l\cdot(c\theta_3 s\theta_1 - c\theta_1 c\theta_2 s\theta_3) & l\cdot(s\theta_1 s\theta_2 s\theta_3) & l\cdot(c\theta_1 s\theta_3 - c\theta_2 c\theta_3 s\theta_1) \\ 0 & l\cdot(c\theta_2 s\theta_3) & l\cdot c\theta_3 s\theta_2 \end{bmatrix} \tag{11} $$

where $r_{p11} = r_{px}$; $r_{p21} = r_{py}$; $r_{p31} = r_{pz}$.

## 4. Optimization and Optimal Results

This section outlines the optimization problem of the MRB with respect to two objectives: mass and induced torque. It is important to note that these objectives are opposing in the optimization process for designing the MRF brake system. To achieve these requirements, the primary focus of the optimization problem is minimizing the mass of the MRB ($m_b$), while ensuring that the maximum braking torque ($T_b$) remains greater than the required torque ($T_{br}$) to generate the desired feedback force. Thus,

Minimize the MRB mass $m_b$:

$$ OBJ_1 = m_b = V_d\rho_d + V_h\rho_h + V_{MRF}\rho_{MRF} + V_c\rho_c + V_s\rho_s $$

Subject to: $T_b \geq T_{br}$

Here, $V_d$, $V_h$, $V_{MRF}$, $V_c$, and $V_s$ represent the volumes of the disc, housing, MRF, coils, and shaft of the MRB employed in the proposed 3D haptic joystick, while $\rho_d$, $\rho_h$, $\rho_{MRF}$, $\rho_c$, and $\rho_s$ represent the densities of the materials used for these components. It is worth noting that the required induced torque is determined based on the maximum desired feedback force in each direction, as expressed by the following equation:

$$ T_{br} = l_{max} F_{max} \tag{12} $$

In this research, the maximum desired feedback force ($F_{max}$) is selected as 20 N, while the handle length ($l_{max}$) is 200 mm. From these, the required induced torque is determined to be 4 Nm. However, a value of 5 Nm is chosen to account for potential inaccuracies in modeling and losses in the magnetic field.

Additionally, the significant dimensions of the MRB, referred to as design variables (*DVs*), are considered for solving the proposed optimization problem in this study. The *DVs* of the MRB include the thickness of the disc ($t_d$), the height and width of the coil ($w_c$, $h_c$), the inner radius of the disc ($R_i$), the inner radius of the tooth ($R_1$), the thickness of the inclined duct ($t_i$), the thickness of the tooth peak ($t_{tp}$), the thickness of the tooth bottom ($t_{tb}$), the distance between the teeth ($d_t$), the height of the tooth ($h_t$), the thickness of the rectangular tooth ($t_{rt}$), the thickness of the thin-wall ($t_w$), and the thickness of the housing ($t_o$ and $t_h$).

To solve the optimization problem stated above, various optimization methods such as the Newton-Raphson method, Quasi-Newton method, Powell method, and PSO method can be used. Among these methods, the PSO (Particle Swarm Optimization) is one of the most effective approaches for solving a single-objective problem with constraints. This method enables a global optimal value with simple initialization conditions and reduces the computational cost in terms of storage memory and time by requiring simple calculation methods. The PSO continuously explores a new search space using swarm behavior to achieve convergence (Zhu, Wang, Wang, & Chen, 2011)

In this study, the PSO is implemented in MATLAB interacting with ANSYS Mechanical APDL to solve the proposed optimization problem of the MRB. To obtain the optimal solution, it is necessary to determine the input design variables mentioned above, the maximum iteration number ($i_{max}$ = 100) and population size (*pop* = 70). Besides, the acceleration coefficient of the individual ($C_1$) and the acceleration coefficient of the population ($C_2$), and the coefficient of inertia ($w$) are basic parameters of PSO. To achieve faster convergence, the constriction factor approach proposed by Clerc and Kenney is employed in this study. The constriction factor approach of particle swarm is determined by formula (Pranava & Prasad, 2013):

$$\chi = \frac{2k}{\left|2-\varphi-\sqrt{\varphi^2-4\varphi}\right|} \quad (13)$$

Here, $k = 1$, system convergence characteristic can be controlled by $\varphi = \varphi_1 + \varphi_2$, $\varphi > 4$; $\varphi_1 = \varphi_2 = 2.05$. So $C_1$, $C_2$, and coefficient of inertia ($w$) are respectively determined as follows: $C_1 = \chi\varphi_1$, $C_2 = \chi\varphi_2$, and $w = \chi$.

In this study, the Parker-62576 commercial lip-seal is used to prevent the MRF from leaking through the shaft gap. Noteworthily, while a small MRF gap size can produce high induced torque, it may also introduce several disadvantages. These include reduced MRB efficiency due to increased energy dissipation, overheating, and inaccurate feedback forces (resulting from a high off-state induced torque). Additionally, a small MRF gap size can raise fabrication costs and complicate the manufacturing process. To mitigate these inherent limitations of the MRB and simplify both design and fabrication, the MRF gap ($d$) is empirically set to 0.8 mm in this study. The copper coil wire utilized in this study has a 24-gauge size, a maximum working current of approximately 3 A, and a diameter of 0.511 mm. To ensure safe working conditions, a current of 2.5 A is provided to the coil during the optimization process, while a filling ratio of 0.7 and a magnetic loss assumption of 10% are respectively chosen based on experimental experience.

After 100 iterations, the optimal solution of the MRBs is obtained at the 10th loop. The optimal results indicate that the mass and induced torque of the MRB are 0.6871 kg and 5.118 Nm, respectively, at the optimum. Figure 4 and Figure 5 illustrate values of objective function ($m_b$) during the optimization process using the PSO method and the magnetic flux density of the MRB at the optimum. The optimized design shows a notable reduction in magnetic density across the MRF duct gap compared to the initial design values. Additionally, the mass and induced torque of the MRB at the optimum (0.6871 kg, 5.118 Nm) are significantly lower than their initial values (2.735 kg, 7.434 Nm). This clearly highlights the substantial improvements in both the structure and performance of the MRB as a result of the optimization process. Simultaneously, the induced torque of the MRB at the optimum (5.118 Nm) satisfies the constraint condition (the required induced torque exceeds 5 Nm). Finally, the optimal results of the MRB used for the proposed 3D haptic joystick are summarized in Table 2.

## 5. Experimental Results

Three MRB prototypes were fabricated based on the optimal results from Table II and incorporated into the proposed 3D haptic joystick. The joystick has three MRBs aligned perpendicularly in each axis, generating feedback forces (Fx, Fy, Fz) for the operator to perceive. The joystick knob is connected to an OptoForce 3D OMD-20-FG-100N force sensor, which measures the forces, with data transferred to a National Instruments (NI)-6001 card via Labview software. The PPW-8011 programming power supplies power to the MRBs and enables the DAQ to adjust the current to the desired level, ranging from 0 to 2.5 A. The incremental encoders are used to determine the angles of the gimbal mechanism in the $X$, $Y$, and $Z$ axes. The operation point position can be determined from the encoder's information ($\theta_1$, $\theta_2$, and $\theta_3$) using equation (9), which relates the knob position to the gimbal angles. The experimental setup is shown in Figure 6, and it enables accurate measurement and control of the feedback forces generated by the MRBs in the 3D haptic joystick.

The experimental results indicate that the off-state torque values for MRB01, MRB02, and MRB03 are 0.64 Nm, 0.62 Nm, and 0.58 Nm, respectively. The discrepancy in the

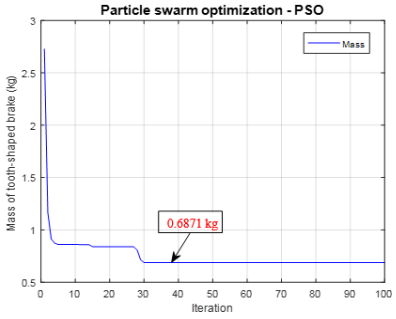


Figure 4. Mass of MRB during the optimization process

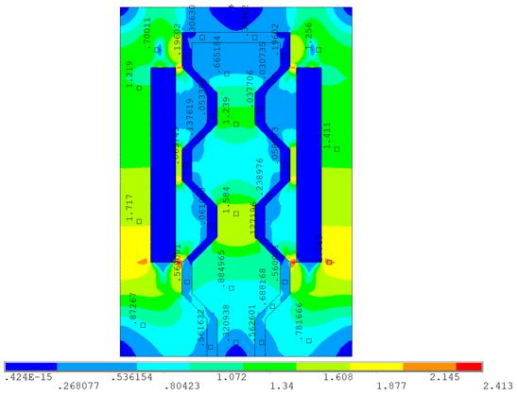


Figure 5. Magnetic distribution of the optimized MRBs

Table 2. Optimal solution of MRBs

| Parameters (mm) | Characteristic |
|---|---|
| $t_d = 3$; $w_c = 2$; $h_c = 15.49$; $R_i = 6$; $R_1 = 9$; $t_i = 2$; $t_{tp} = 2.5$; $t_{tb} = 2.49$; $d_t = 6.49$; $h_t = 2$; $t_{rt} = 2$; $t_w = 0.5$; $t_o = 2$; $t_h = 2.43$; $L = 23.07$; $R = 33.79$ | Mass: $m_b = 0.6871$ kg<br>Off-state torque: $t_{b0} = 0.022$ Nm<br>Induced torque: $T_b = 5.118$ Nm<br>Power consumption: 17.197 W<br>Number of turns of wire: 122<br>Coil resistant: 2.75Ω |

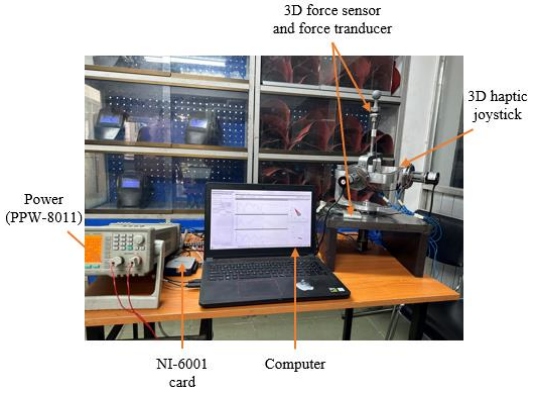


Figure 6. Experimental setup for the prototype of the 3D haptic joystick

values could be attributed to various factors, such as inaccuracies in the fabrication and assembly process, incorrect material property inputs, or a lack of actual turns of wire. The numbers of turns for MRB01, MRB02, and MRB03 are 116, 116, and 120, respectively. At a current of 2.5 A, the feedback torque values for these MRBs are 3.96 Nm, 3.95 Nm, and 4.1 Nm, respectively. The difference between the measured and desired values is approximately 20% when compared to the required maximum torque on each side. However, the induced torque for the MRBs used in the proposed joystick satisfies the condition of 4 Nm. Figure 7 illustrates the feedback torque of these MRBs for the proposed joystick from 0 to 2.5 A. The response time for the induced output torque, which includes both the mechanical and induced output torque response times for MRB01, MRB02, and MRB03, is approximately 0.52 s, 0.56 s, and 0.55 s, respectively.

By analyzing Figure 7, the correlation between the applied current to the coil and the induced torque of the magnetorheological brakes (MRBs) can be clearly identified. To quantify this relationship, curve fitting methods are applied to the data in Figure 8, enabling the estimation of the required current for MRB01, MRB02, and MRB03 using Equations (14), (15), and (16), respectively. A comparison between experimental and simulation results indicates that the braking torque responses to changes in current are nearly identical. This demonstrates the high accuracy of the simulation model in predicting the working characteristics of the brake, validating its use for performance evaluation and optimization before conducting real-world experiments. Furthermore, these findings confirm that the induced torque of the brake can be effectively controlled by adjusting the applied current. Finally, from Equation (12), the feedback force of the joystick can be determined, allowing for a more precise assessment of the system's force control capabilities.

$$T_x = 0.512473 + 1.07495I + 0.164581I^2 \quad (14)$$

$$T_y = 0.5043 + 0.83857I + 0.207804I^2 \quad (15)$$

$$T_z = 0.291577 + 1.73936I + 0.0695055I^2 \quad (16)$$

## 6. Conclusions

This study proposes a force-feedback 3D joystick mechanism as an active master to control passive slave devices. After reviewing related studies and their limitations, the proposed configuration aims to address their shortcomings. MRBs are used to generate feedback force, with a new MRB design developed and optimized using PSO and the finite element method. The optimal MRB results show a mass of 0.6871 kg and induced torque of 5.118 Nm, meeting the optimization and feedback force requirements. The kinematics of the joystick are presented to determine the knob position. Prototypes of the MRBs, based on the optimal results, are fabricated and assembled to generate feedback forces along the X, Y, and Z axes. Experimental results show that the MRBs (MRB01, MRB02, MRB03) produce feedback torques of 3.96 Nm, 3.95 Nm, and 4.1 Nm at 2.5 A, with the current-feedback force relationship determined through curve fitting.

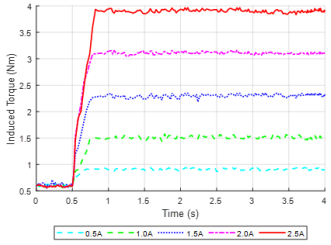


(a) Induced torque of MRB03 (MRB_X)

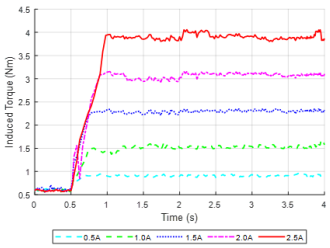


(b) Induced torque of MRB02 (MRB_Y)

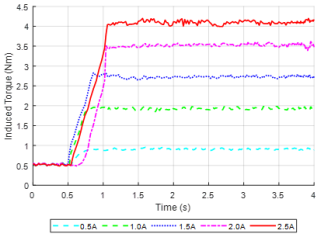


(c) Induced torque of MRB01 (MRB_Z)

Figure 7. Experimental results of prototype MRBs in response to applied current

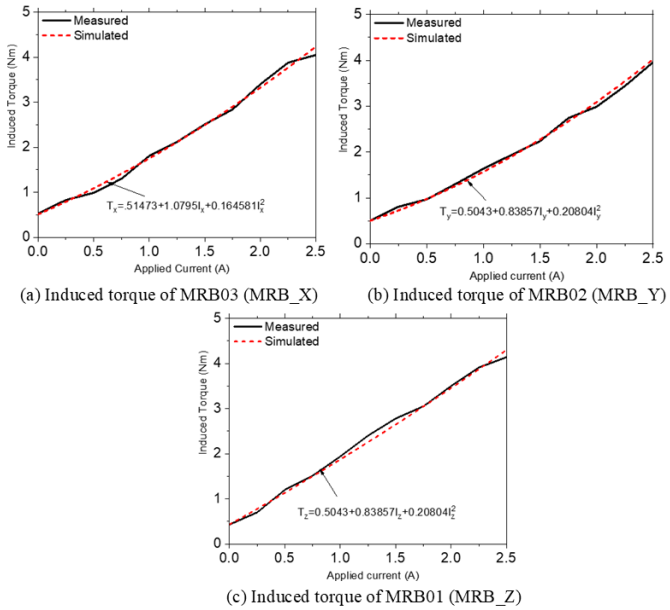


Figure 8. The relationship between induced torque and applied current

In future research, a multi-objective optimization of the MRB will be conducted to reduce mass, off-state torque, and power consumption. Additionally, a controller for the proposed joystick will be introduced.

## Acknowledgements

This research is funded by Industrial University of Ho Chi Minh City under grant number 129/HĐ-ĐHCN.

## References

Bullion, C., & Gurocak, H. (2009). Haptic glove with MR brakes for distributed finger force feedback. *Journals and Magazines: Presence*, *18*(6), 421-433. doi:0.1162/pres.18.6.421.

Choi, S. H., Kim, S., Kim, P., Park, J., & Choi, S. B. (2015). A new visual feedback-based magnetorheological haptic master for robot-assisted minimally invasive surgery. *Smart Materials and Structures*, *24*(6). 065015. doi: 10.1088/0964-1726/24/6/065015.

Diep, B. T., Nguyen, Q. H., Kim, J. H., & Choi, S. B. (2020). Performance evaluation of a 3D haptic joystick featuring two bidirectional MR actuators and a linear MRB. *Smart Materials and Structures*, *30*(1). doi: 10.1088/1361-665X/abc668.

Kang, B. H., Kim, B. G., Jung, D., & Choi, S. B. (2022). A mathematical model of cavitation behavior in a single-ended magnetorheological damper: experimental validation. *Smart Materials and Structures*, *31*(3). doi:10.1088/1361-665X/ac4cdd.

Kim, P., Kim, S., Park, Y. D., & Choi, S. B. (2016). Force modeling for incisions into various tissues with MRF haptic master. *Smart Materials and Structures*, *25*(3), 035008. doi: 10.1088/0964-1726/25/3/035008.

Nguyen, N. D., Thang, L. D., & Nguyen, Q. H. (2018). Development of new magnetorheological fluid-based brake with multiple coils placed on the side housings. *Journal of Intelligent Material Systems and Structures*, *30*(5), 734-748. doi:10.1177/1045389X18818385.

Nguyen, P. B., Oh, J. S., & Choi, S. B. (2012). A novel 2-DOF haptic master device using bi-directional magneto-rheological brakes: Modelling and experimental investigation. *International Journal of Materials and Product Technology*, *44*(3-4), 216-226. doi:10.1504/IJMPT.2012.050191.

Nguyen, Q. H., & Choi, S. B. (2012). Optimal design of novel hybrid MR brake for motorcycles considering axial and radial magnetic flux. *Smart Materials and Structures*, *21*(5). doi:10.1088/0964-1726/21/5/055003.

Nguyen, Q. H., Choi, S. B., Lee, Y. S., & Han, M. S. (2013). Optimal design of a new 3D haptic gripper for telemanipulation, featuring magnetorheological fluid brakes. *Smart Materials and Structures*, *22*(1). doi:10.1088/0964-1726/22/1/015009.

Nguyen, Q. H., Hiep, L. D., Duy, B. Q., & Choi. S. B. (2016). Development of a new clutch featuring MR fluid with two separated mutual coils. In V. Duy, T. Dao, I. Zelinka, HS. Choi, & M. Chadli. (Eds.), *Lecture Notes in Electrical Engineering: Volume 371. Advances in Electrical Engineering and Related Sciences* (pp.835-844). Cham, Germany: Springer. doi:10.1007/978-3-319-27247-4_69.

Oh, J. S., Choi, S. H., & Choi, S. B. (2014). Design of a 4-DOF MR haptic master for application to robot surgery: virtual environment work. *Smart Materials and Structures*, *23*(9). doi:10.1088/0964-1726/23/9/095032.

Pranava, G., & Prasad, P. V. (2013). Constriction coefficient particle swarm optimization for economic load dispatch with valve point loading effects. *2013 International Conference on Power, Energy and Control (ICPEC)*, 350-354. doi:10.1109/ICPEC.2013.6527680.

Senkal, D., & Gurocak, H. (2009). Spherical brake with MR fluid as multi degree of freedom actuator for haptic. *Journal of Intelligent Material Systems and Structures*, *20*(18), 2149-2160. doi:10.1177/1045389X09348925.

Varela-Jiménez, M. I., Vargas Luna, J. L., Cortés-Ramírez, J. A., & Song, G. (2015). Constitutive model for shear yield stress of magnetorheological fluid based on the concept of state transition. *Smart Materials and Structures*, *24*(4). doi:10.1088/0964-1726/24/4/045039.

Winter, S. H., & Bouzit, M. (2007). Use of Magnetorheological fluid in a force feedback glove. *Journals and Magazines: IEEE Transactions on Neural Systems and Rehabilitation Engineering*, *15*(1), 2-8. doi:10.1109/TNSRE.2007.891401.

Yamaguchi, Y., Furusho, J., Kimura, S., Koyanagi, K. (2004). High-performance 2-D force display system using MR actuators. *IEEE/RSJ International Conference on Intelligent Robots and Systems (IROS), Volume 3*, pp.2911-2917. Sendal, Japan. doi:10.1109/IROS.2004.1389851.

Zhu, H., Wang, Y., Wang, K., & Chen, Y. (2011). Particle Swarm Optimization (PSO) for the constrained portfolio optimization problem. *Expert Systems with Applications*, *28*(8), 10161-10169. doi:10.1016/j.eswa.2011.02.075.